Limits on the Isolation of Stochastic Vibration for Microgravity Space Experiments

C. R. Knospe* and P. E. Allaire†
University of Virginia, Charlottesville, Virginia 22901

The limitations on the isolation of stochastic vibrations for microgravity space experiments are explored. These limitations result from the restricted interior space available for vibration isolation. A one-degree-of freedom representation of the experiment-spacecraft system is used, and an ideal vibration actuator is assumed. A kinematic representation results, and the problem becomes one of finding the minimum acceleration trajectory within a pair of stochastic walls. The wall motion is characterized by an ergodic, stationary, zero-mean, Gaussian random process with known power spectral density. The geometry of the wall trajectories is defined in terms of their significant extrema and zero crossings. This geometry is used in defining a composite trajectory that has a mean square acceleration lower than that on the optimal path satisfying the stochastic wall inequality constraints. The optimal control problem is solved on a return path yielding the mean square acceleration in terms of the distributions of significant maxima and first-passage time of the wall process. The methodology is applied to a microgravity isolation problem to find the lower bounds on root-mean-square acceleration given the disturbance power spectral density.

Nomenclature

A = matrix in state dynamics
$\boldsymbol{B}$ = vector in state dynamics
c_i = constants in optimal control
d = microscopic component of $y(t)$
F = cumulative distribution function
f = probability density function
G = final condition cost
$G(s)$ = transfer function of shaping filter
H = Hamiltonian
J = cost function
L = maximum stroke of experiment
m_{-4} = fourth moment of a sample of T^{-1}
n = bandlimited white noise
S = power spectral density.
s = complex frequency variable
T = first-passage time
t = time
t_1 = time at significant maximum
t_2 = time at zero crossing
u = experiment acceleration
$\boldsymbol{x}$ = state vector, $= (x_1\ x_2)^T$
x, x_1 = experiment position
x_2 = experiment velocity
y = wall process
y_1 = upper wall true position
y_2 = lower wall true position
y_{up} = upper wall constraint
y_{low} = lower wall constraint
y_{max} = maximum of wall process
$\bar{y}, \bar{y}_1$ = macroscopic component at $y(t)$
$\bar{y}_2$ = macroscopic component velocity
z = significant maximum position
δ = dirac delta function
λ_i = Lagrange multiplier for dynamic equations
ϕ = Lagrange multiplier for final condition
ν = expected frequency of upcrossings (cycles)
μ = expected frequency of maxima
ω = frequency, rad/s
ω_d = damped natural frequency, rad/s
ξ = damping coefficient

Subscripts

d = microscopic component
f = final time
max = at maximum
N = normal
n = bandlimited white noise
T = first-passage time
y = wall process
$\bar{y}$ = macroscopic component
z = significant maxima position

Introduction

THE microgravity environment of space may permit advances in material science experiments. Such experiments could aid in the understanding of basic physical phenomena, quantify the limitations and effects imposed by gravity, and spur application to Earth and space based processes and products. A microgravity environment could potentially eliminate buoyancy-driven convection, sedimentation, and hydrostatic pressure as well as yield other advantages.[1]

At this time, the acceleration environment requirements for various experiments are not well known.[2] An assessment of existing theoretical and experimental data available up to 1985 indicated acceleration levels below $10^{-6}\ g_0$ would be required for frequencies below 0.1 Hz for many of the processes. The requirements at higher frequencies are somewhat lower.[3] Work to determine the levels necessary is in progress by various materials experiment researchers. An example is a twin crystal growth experiment to be carried out on spacecraft.[4]

An essential part of the development of a microgravity experiment program is the characterization of the low acceleration environment aboard spacecraft. NASA has carried out a series of measurements reported at various

Received June 29, 1990; revision received Aug. 21, 1990; accepted for publication Sept. 10, 1990.

*Assistant Research Professor, Department of Mechanical and Aerospace Engineering.
†Professor, Department of Mechanical and Aerospace Engineering.

Table 1 Microgravity space experiment acceleration environment[7]

g/g_0	F, Hz	Source
	Quasisteady or "dc" acceleration disturbances	
10^{-7}	0 to 10^{-3}	Aerodynamic drag
10^{-8}	0 to 10^{-3}	Light pressure
10^{-7}	0 to 10^{-3}	Gravity gradient
	Period acceleration disturbances	
2×10^{-2}	9	Thruster fire (orbital)
2×10^{-3}	5-20	Crew motion
2×10^{-4}	17	Ku band antenna
	Nonperiodic acceleration disturbances	
10^{-4}	1	Thruster fire (attitude)
10^{-4}	1	Crew push off

conferences.[5,6] A summary of this data was presented in Ref. 7 and is repeated in Table 1. Additional results have been reported in Refs. 8 and 9.

The vibration levels reported in the above literature for spacecraft are significantly greater than allowable for material science experiments. In order to achieve accurate and reproducible results in such experiments, vibration isolation will be required.[3] Acceleration disturbances in the orbiter environment cover a wide frequency bandwidth, from 0 to 100 Hz. Sources include spacecraft drag, light pressure oscillations, manned activity, and thruster fire. The frequency and amplitudes of these accelerations are summarized in Table 1.

The frequency and amplitude of any particular vibration source determines the level of isolation that can be achieved. At relatively high frequencies, above approximately 10 Hz, passive vibration isolation is normally possible. Two examples of such isolation systems are reported in Refs. 10 and 11. For lower frequencies, active vibration isolation is necessary. One of the few such systems is examined in Ref. 12.

A fundamental restriction on active microgravity vibration isolation systems is the limited available volume aboard spacecrafts for experiments. This kinematic constraint cannot be overcome through improvement of the vibration isolation control system, sensors, or actuator. The purpose of this paper is to explore the limitations on vibration isolation systems arising from the stroke restriction. Thus an ideal vibration actuator is assumed, and the problem is solved in part by optimal control theory. This work is an extension of research on isolation limits under sinusoidal excitation.[13] In this paper, the excitation is a wideband, zero-mean stochastic process. A lower bound on the root-mean-square acceleration is determined in terms of the maximum stroke.

Optimal Control Formulation

While the isolation problem for microgravity space experiments is multidimensional, this analysis examines the one-dimensional case. Consider the system illustrated in Fig. 1 with experiment position $x(t)$ and wall positions $y_1(t)$ and $y_2(t)$. The experiment is connected to the spacecraft by umbilicals, such as power or fluid lines, and by a vibration isolation actuator. Although the spacecraft has a finite mass, it may be considered to have infinite impedance for this analysis since the spacecraft-to-experiment weight ratio is very large. The spacecraft acts as an external base motion transmitting forces through the umbilical and the actuator.

An ideal actuator is assumed. Therefore, the acceleration of the experiment is the minimum acceleration possible given that the experiment stay between the two walls. The effects of the power/data/cooling umbilicals represented in Fig. 1 are removed through the ideal actuator. Thus, the problem is reduced to a kinematic representation. The vibration isolation problem becomes an optimal control problem: find the optimal trajectory (minimum acceleration) given the constraint conditions (moving walls). This problem formulation was used previously by the authors to find the limitations on isolation for harmonic disturbances.[13]

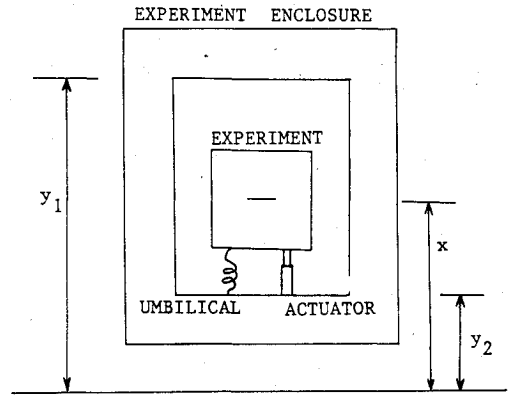

Fig. 1 One-degree-of-freedom isolation problem.

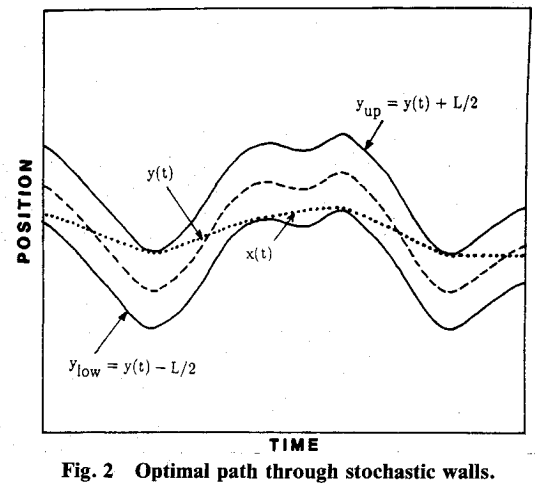

Fig. 2 Optimal path through stochastic walls.

Significant Extrema

The kinematic formulation allows the stochastic problem to be easily conceived. Figure 2 illustrates. An optimal trajectory $x(t)$ is sought between two walls whose motion is described by a single zero-mean stochastic process $y(t)$,

$$y_{up} = y(t) + L/2$$

$$y_{low} = y(t) - L/2$$

where L is the maximum stroke of the experiment between the two walls.

Let the experiment acceleration be denoted as $u(u = \ddot{x})$. Then the cost function J to be minimized is

$$J = \int_0^\infty u^2 \, dt \tag{1}$$

with the constraint

$$y(t) - \frac{L}{2} \le x(t) \le y(t) + \frac{L}{2}, \qquad 0 \le t \tag{2}$$

for a given wall centerline motion $y(t)$. The optimal trajectory will be in general smooth with as few extrema as possible. The trajectory will also cover as little distance as possible. As previously reported in Ref. 13, with a sinusoidal disturbance, the optimal trajectory tangents the maxima of the lower wall and the minima of the upper wall when the amplitude of $y(t)$ is greater than $L/2$. Given these tangencies, it is an easy task to compute the minimum acceleration path connecting them. Although this path may intersect a wall's path, as was reported in Ref. 13, this "cheating" results in less than a 1% reduction in root-mean-square from the true optimal path. By dropping the inequality constraints from the optimal control problem

and replacing them with the tangency conditions at the wall's extrema, a tight lower bound on the minimum root-mean-square acceleration is obtained. This is the approach taken here with the stochastic problem. For this analysis, the wall process $y(t)$ and its derivatives are assumed to be stationary, zero-mean, Gaussian random processes.

Once again, the wall inequality constraints are ignored and are replaced with interior point equality conditions. A tangency condition is assumed at some of the walls' extrema and the trajectory is required to cross zero at the same time as $y(t)$. This last requirement is made to ensure a tight lower bound. Note that a zero crossing of $x(t)$ must occur at or before $y(t)$ leaves the $\pm L/2$ interval. However, for most random processes $y(t)$, the additional requirement of simultaneous zero crossing results in a realistic and tighter lower bound. The upper wall is ignored as a constraint when $y(t) > 0$ as the lower wall is when $y(t) < 0$. Thus, only upper wall minima when $y(t) < 0$ and lower wall maxima when $y(t) > 0$ are eligible tangency condition points. Figure 3 illustrates this geometry and a composite path connecting the prescribed interior points. The optimal composite trajectory satisfying these interior point equality constraints will have a root-mean-square acceleration lower than that of the optimal trajectory satisfying the original inequality constraints under almost all conditions. Note that the composite trajectory is not required to have first derivative continuity at the interior zero crossing points. (It will, of course, have a continuous first derivative at the extrema tangent points.) It should be pointed out that the composite trajectory is not intended to be an implementable optimal control path; the trajectory is a theoretical tool to investigate the limitations on vibration isolation.

Not all eligible lower wall maxima and upper wall minima will be tangented by the optimal composite trajectory. In Fig. 4, note that if $|y(t)| < L/2$, as shown on the left side of the figure, the optimal path is $x(t) = 0$. However, if the eligible extremum crosses zero (i.e., if $|y(t)| > L/2$) as on the right side, the optimal composite path must depart from $x(t) = 0$ to avoid collision with the wall.

Because of the wideband character of the stochastic wall acceleration, many extrema tend to be clustered at every peak of $y(t)$. The composite trajectory will only tangent one of these extrema and that only if $|y(t)| > L/2$. The effort here is to distinguish the extrema which the composite trajectory needs to include (in order to be a useful lower bound) from the bulk of immaterial extrema.

A wall extremum in a time interval that requires an increase in the cost function during the interval is classified here as a significant extremum. (This is, admittedly, not a rigorous definition; however it satisfies the purpose of this investigation.) The optimal composite path, therefore, runs between significant extrema and $y = 0$. The composite path is a combination of paths of the experiment at rest, departing to an extremum, and returning from an extremum as indicated in Fig. 4. Each of these cases can be analyzed in terms of a return path. [Departing paths are kinematically the same as returning paths since the random processes $y(t)$ and $\dot{y}(t)$ are independent since they are Gaussian. A rest path is equivalent to a return path when $|y(t)| < L/2$.] By finding the expected value of the mean square acceleration on a return path, the mean square acceleration of the composite path is determined, and a lower bound is set on the optimal trajectory mean square acceleration. Thus, a lower bound is found by characterizing the distribution of the significant extrema in time and position.

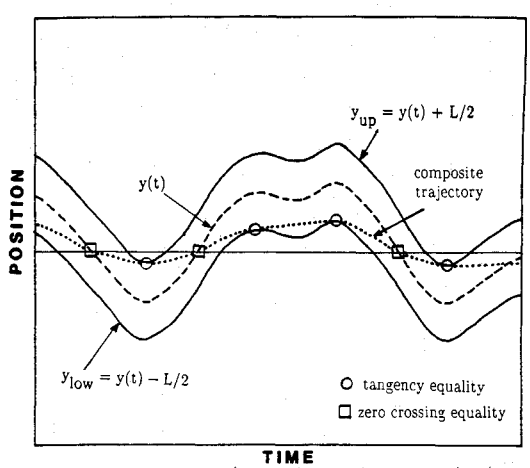

Fig. 3 Stochastic walls, interior point equality conditions, and composite trajectory.

Solution in Terms of the Significant Extrema

The return path and its mean square acceleration given a significant extremum is now found. Examine the time history shown in Fig. 5. The optimal path during the interval (t_1, t_2) satisfying the wall inequality constraints over a much larger interval has, in general, a root-mean-square acceleration bounded below by the root-mean-square acceleration on the return path connecting points 1 and 2. [This will be true for all but wideband $y(t)$ processes with large maximum stroke, L. Note that $\ddot{y}(t)$ can be wideband with $y(t)$ not.] The boundary constraints at these two points for the return path are

$$x(t_1) = z \qquad x(t_2) = 0$$
$$\dot{x}(t_1) = 0 \qquad \dot{x}(t_2) = \text{free} \tag{3}$$

where $z = y_{max} - L/2$.

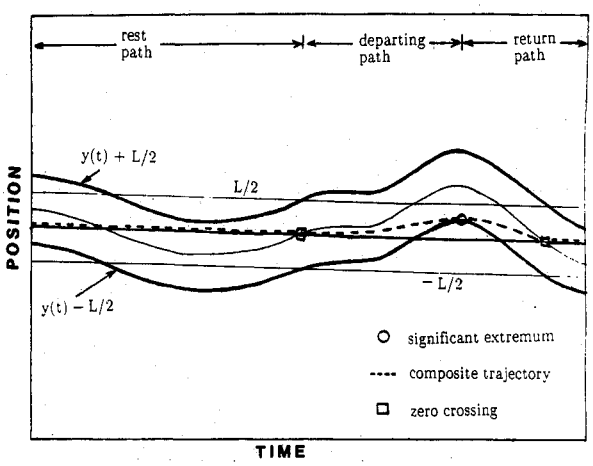

Fig. 4 Significant extrema and composite trajectory.

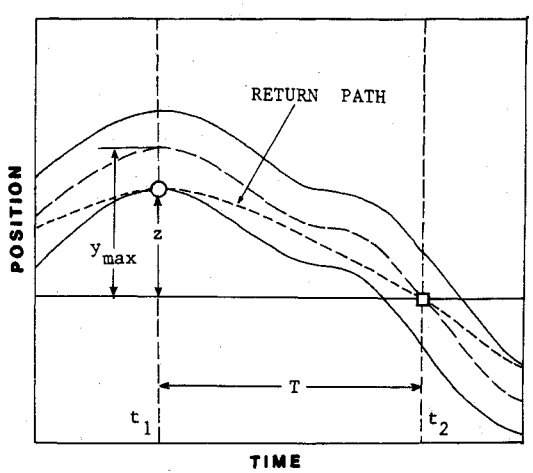

Fig. 5 Significant maximum, return path, and boundary conditions.

The velocity boundary condition at time t_2 is left free since this condition depends on the next significant extremum, the location of which cannot be readily derived even in a probabilistic sense. Therefore, the velocity at time t_2 is unspecified so that the return path root-mean-square acceleration will be a lower bound on the minimum acceleration. The optimal control problem is thus reduced to that over the time t_1 to t_2 with cost function

$$J = \int_{t_1}^{t_2} u^2 \, dt \tag{4}$$

and the boundary conditions of Eq. (3).

This problem is solved by the calculus of variations (Appendix A) yielding the optimal trajectory.[14]

The mean-square acceleration on this trajectory is

$$MS(\ddot{x}) = \left[\frac{1}{(t_2 - t_1)} \int_{t_1}^{t_2} u^2 \, dt\right] = \frac{3z^2}{T^4} \tag{5}$$

where $T = (t_2 - t_1)$, the time from significant extrema to zero crossing, or the first-passage time. This is the lower bound sought. Assuming that the wall process $y(t)$ is ergodic, the minimum mean square experiment acceleration attainable with an ideal isolator must be greater than the mean-square acceleration of the composite trajectory,

$$E\left\{\frac{3z^2}{T^4}\right\}$$

where $E\{\cdot\}$ is the exact value operator[15]

$$E\left\{\frac{3z^2}{T^4}\right\} = \int_0^\infty \int_0^\infty \frac{3z^2}{T^4} f_{zT}(z,t) \, dz \, dT \tag{6}$$

Here, $f_{zT}(\cdot,\cdot)$ is the joint probability density function on the significant maxima z, and the time from significant maxima to zero crossing T. (The significant extrema problem can be solved for in terms of significant maxima because of the symmetry of the problem.) Equation (6) can be rewritten

$$E\left\{\frac{3z^2}{T^4}\right\} = \int_0^\infty 3z^2 f_z(z) \, E\left\{\frac{1}{T^4} | z\right\} dz \tag{7}$$

where $E\{(1/T^4)|z\}$ is the conditional fourth moment of T^{-1}, and $f_z(\cdot)$ is the probability density function of the significant maxima.

Distribution of Significant Maxima

Consider the stationary, zero-mean, Gaussian random process describing the wall's acceleration $\ddot{y}(t)$. This process can be characterized by its power spectral density $S_{\ddot{y}}(\omega)$.[16] The mean square of the wall acceleration is the integral of this over frequency[17]

$$E(\ddot{y}^2) = \sigma_{\ddot{y}}^2 = \int_{-\infty}^{\infty} S_{\ddot{y}}(\omega) \, d\omega \tag{8}$$

(simply the area underneath the power spectral density curve). The mean square of the velocity and position processes are

$$E(\dot{y}^2) = \sigma_{\dot{y}}^2 = \int_{-\infty}^{\infty} \frac{S_{\ddot{y}}(\omega)}{\omega^2} \, d\omega \tag{9}$$

$$E(y^2) = \sigma_y^2 = \int_{-\infty}^{\infty} \frac{S_{\ddot{y}}(\omega)}{\omega^4} \, d\omega \tag{10}$$

For a Gaussian process, the density of upcrossings of $y = 0$ for the $y(t)$ process[15,18] is

$$\nu_y = \frac{\sigma_{\dot{y}}}{2\pi\sigma_y} \tag{11}$$

and the density of maxima of $y(t)$ is

$$\mu_y = \frac{\sigma_{\ddot{y}}}{2\pi\sigma_{\dot{y}}} \tag{12}$$

Rice[19] and Houston and Skopinski[20] have shown that the probability density function for the distribution of the maxima of a stationary Gaussian random process is dependent only on the ratio μ_y/ν_y and the standard deviation of the process σ_y

$$f_{y_{\max}}(y/\sigma_y) = (1 - \nu_y^2/\mu_y^2)^{1/2} f_N\left[\frac{y/\sigma_y}{(1-\nu_y^2/\mu_y^2)^{1/2}}\right] + (2\pi)^{1/2} \frac{\nu_y}{\mu_y}\left(\frac{y}{\sigma_y}\right) f_N\left[\frac{y}{\sigma_y}\right] F_N\left[\frac{y/\sigma_y}{(\mu_y^2/\nu_y^2 - 1)^{1/2}}\right] \tag{13}$$

where f_N and F_N are the normal probability density function and its integral

$$f_N(x) = (2\pi)^{-1/2} e^{-(x^2/2)}$$

$$F_N(x) = \int_{-\infty}^{x} f(a) \, da \tag{14}$$

(Lin[21] has an interesting discussion on this maxima distribution.)

The ratio μ_y/ν_y can be regarded as the average number of maxima between upcrossings for the $y(t)$ process.[18] Probability density functions for the distribution of maxima of a stationary Gaussian random process are shown for different values of this ratio in Fig. 6.

A random wall process typical of the microgravity vibration environment will have many maxima per zero crossing ($\mu_y/\nu_y \gg 1$). Most of these maxima are clustered near the peaks of the process and can be considered the high frequency component.[18] Figure 7 illustrates. The random process $y(t)$, as was shown by Crandall,[18] can be decomposed into the sums of a macroscopic component $\bar{y}(t)$ and a microscopic component $d(t)$

$$y(t) = \bar{y}(t) + dt \tag{15}$$

The macroscopic component has a much smaller root mean square σ_d and greater frequency of zero crossing ν_d than the macroscopic signal ($\sigma_{\bar{y}}$, $\nu_{\bar{y}}$). The macroscopic component will have nearly the same amplitude as the original signal. The distribution of maxima given in Eq. (13) is the distribution of both the micromaxima and macromaxima. Clearly, the micromaxima do not contribute (substantially) to the cost

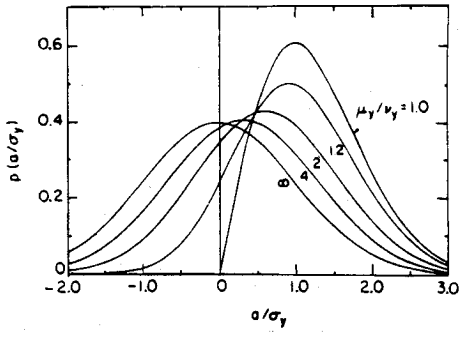

Fig. 6 Probability density function for the distribution of maxima of a stationary Gaussian process.

function; therefore, they are, by definition, not significant maxima.

The distribution of significant maxima is therefore derived from the distribution of macromaxima, the maxima of the $\bar{y}(t)$ process,

$$f_{\bar{y}_{\max}}(\bar{y}/\sigma_{\bar{y}}) = (1-\nu_{\bar{y}}^2/\mu_{\bar{y}}^2)^{1/2} f\left[\frac{\bar{y}/\sigma_{\bar{y}}}{(1-\nu_{\bar{y}}^2/\mu_{\bar{y}}^2)^{1/2}}\right] + (2\pi)^{1/2}\frac{\nu_{\bar{y}}}{\mu_{\bar{y}}}\left(\frac{\bar{y}}{\sigma_{\bar{y}}}\right) f_N\left[\frac{\bar{y}}{\sigma_{\bar{y}}}\right] F\left[\frac{\bar{y}/\sigma_{\bar{y}}}{(\mu_{\bar{y}}^2/\nu_{\bar{y}}^2-1)^{1/2}}\right] \tag{16}$$

To obtain the density function for the distribution of significant maxima from the distribution of macromaxima it is only necessary to recall Eq. (3) with $\bar{y}_{\max}$ replacing $y_{\max}$

$$z = \begin{cases} \bar{y}_{\max} - L/2 & \bar{y}_{\max} > L/2 \\ 0 & \bar{y}_{\max} < L/2 \end{cases} \tag{17}$$

find the cumulative distribution on z in terms of the cumulative distribution on $\bar{y}_{\max}$

$$F_z(z) = \begin{cases} F_{\bar{y}_{\max}}(z + L/2) & z > 0 \\ 0 & z < 0 \end{cases} \tag{18}$$

and to differentiate with respect to z[15]

$$f_z(z) = \begin{cases} F_{\bar{y}_{\max}}(L/2)\delta(z) + f_{\bar{y}_{\max}}(z + L/2) & z > 0 \\ 0 & z < 0 \end{cases} \tag{19}$$

where $\delta(\cdot)$ is the dirac delta function. Note that the portion of the $\bar{y}_{\max}$ distribution between $-\infty$ and $L/2$ maps into a dirac delta at $z = 0$. The integration of this part of $f_z(z)$ in Eq. (7) will be zero

$$\int_0^\infty 3z^2 F_{\bar{y}_{\max}}(L/2)\,\delta(z)\,E\left\{\frac{1}{T^4}\middle| z\right\} dz = 0 \tag{20}$$

The nonsignificant maxima, therefore, do not increase the expected mean square. (Note that $E\{(1/T^4)|z=0\}$ is finite since T is defined as the time for the $\bar{y}(t)$ process to reach $\bar{y}=0$ starting from rest at $y_{\max}$. When $z=0$, $\bar{y}_{\max} = L/2$; therefore, T is greater than zero.)

The tightness of the lower bound on experiment mean square acceleration given in Eq. (7) depends on the accuracy of the geometric configuration, Fig. 5, in representing typical wall position histories. The decomposition, or smoothing, of the $y(t)$ process yields a macroscopic random process $\bar{y}(t)$ upon which to base the lower bound. If the random process $\bar{y}(t)$ has close to one maxima per upcrossing on average (it must have at least one since it is continuous), the typical geometric configuration will resemble Fig. 5. Thus, for a narrowband random process $\bar{y}(t)$, the bound will be very tight. (In the limit this approaches a sinusoid with slowly changing random amplitude and phase[22]; the resulting bound would be only a few percent low.) For a wideband macroscopic process the bound will be considerably looser but non-trivial. It is therefore desirable that the decomposition produce a macroscopic process with an average number of maxima per upcrossing ($\mu_{\bar{y}}/\nu_{\bar{y}}$) close to one. The smoothed process $\bar{y}(t)$ should also have nearly the same variance as the original signal $\bar{y}(t)$. A method for the decomposition of $\bar{y}(t)$ and $d(t)$ will be discussed later with the application.

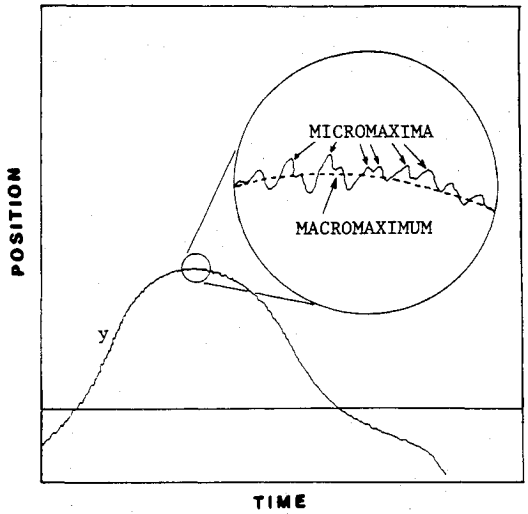

Fig. 7 Macroscopic maxima and microscopic maxima.

First-Passage Problem

An expression for $E\{(1/T^4)|z\}$ can be found explicitly if the conditional probability density function $f_T(T|z)$ is known[15]

$$E\{(1/T^4)|z\} = \int_0^\infty \frac{1}{T^4} f_T(T|z)\, dT \tag{21}$$

The distribution of the first passage time of a stochastic process T is a classical problem probability that has been tackled with limited success by many authors.[23-25] No exact theoretical solution exists. Many approximate methods have been used including series solution,[23] Poison approximation,[24] numerical probability diffusion, and Monte Carlo techniques.[25] The particular variant of the first-passage problem of interest here is nonstationary due to its initial conditions

$$\bar{y}(t_1) = \bar{y}_{\max}$$
$$\dot{\bar{y}}(t_1) = 0 \tag{22}$$

and can be expected to have a crossing in the near future since $\bar{y}(t)$ is zero mean (This, in contrast to the first passage of a level $\bar{y} = a \gg \sigma_{\bar{y}}$, which will occur extremely infrequently.) The nonstationary, quick-crossing nature of this problem suggests Monte Carlo simulation as the preferred method of solution. It is not necessary to generate the conditional probability density function of T in this manner; only the $E\{(1/T^4)|z\}$ is needed.

To perform the simulation, a forced differential equation with the proper probabilistic characteristics must be found. More specifically, the wall acceleration in the simulation should have a power spectral density that matches that of the acceleration disturbance found aboard the spacecraft in the region where the experiment is to be located. Given a measured power spectral density, the dynamic model, or shaping filter, that transforms Gaussian white noise to the desired random process can be found by spectral factorization.[17,26] This dynamic model can then be used in Monte Carlo simulation (Appendix B).

Application to Microgravity Vibration Isolation

The method described above is now applied to the microgravity problem. As described in Ref. 7, vibration aboard spacecraft is essentially of two frequency regions: $0\text{-}10^{-3}$ Hz and above 1 Hz. Consequently, the power spectral density for analysis here is modeled independently in these two regions. The low frequency portion was not obtained from an experimental power spectral density since such information is unavailable. This part of the spectral density, illustrated in Fig. 8, has therefore been devised for the purpose of this example to fit the known environmental disturbances in this

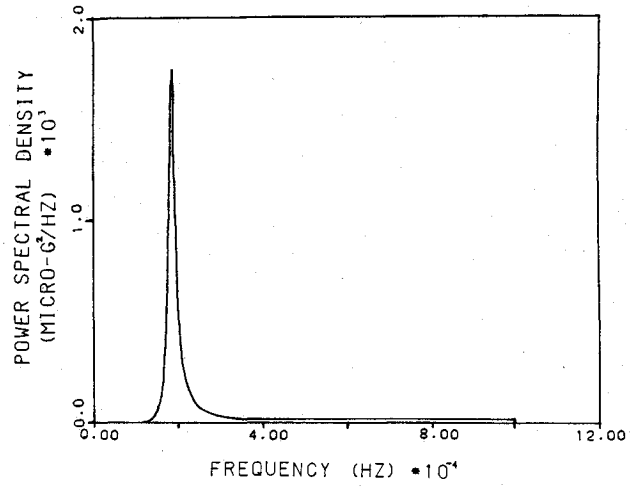

Fig. 8 Acceleration power spectral density in the low frequency range.

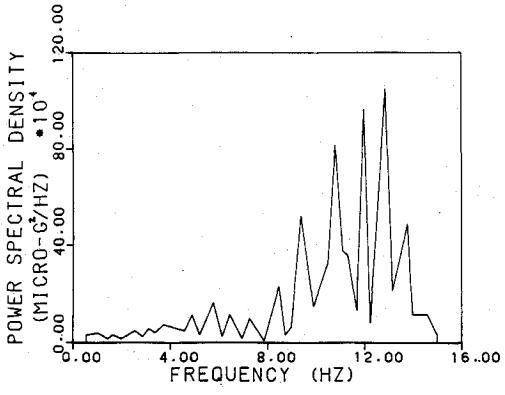

Fig. 9 Acceleration power spectral density in the high frequency range.

frequency range. The spectral density of the analytical model

$$S_{\ddot{y}}(\omega^2) = \begin{cases} \dfrac{75.75\ \omega^4}{(\omega/0.00116)^4 - 1.99\ (\omega/0.00116)^2 + 1} & 0 \le \omega \le 0.006283 \\ 0 & 0.006283 < \omega < 3.14159 \end{cases} \tag{23}$$

has most of its power concentrated near orbital frequency (1.851×10^{-4} Hz, 90 min orbit) with a power corresponding to a root-mean-square acceleration of approximately 0.2 μg. It should be pointed out that the accuracy of the lower bounds generated by this method depends heavily upon the model used in this region.

The high frequency region of the power spectral density, shown in Fig. 9, is from experiments aboard Spacelab.[33] An analytical model could easily be fitted to the curve shown; however, this is not necessary for this application. Note that the method of analysis described previously does not require that disturbance spectral density occupy two separate regions as in this case.

The mean square wall process acceleration, velocity, and position can be found by evaluating Eqs. (8-10) respectively. This may be done through numerical quadrature yielding,

$$\sigma_{\ddot{y}} = 0.016143511 \text{ m/s}^2$$

$$\sigma_{\dot{y}} = 0.0019532654 \text{ m/s}$$

$$\sigma_y = 1.6503623 \text{ m} \tag{24}$$

and by Eqs. (11) and (12)

$$\nu_y = 0.18836582 \times {}^{-3} \text{ upcrossings/s}$$

$$\mu_y = 0.13153971 \times 10^1 \text{ maxima/s}$$

$$\mu_y/\nu_y = 6983.2 \text{ maxima/upcrossing} \tag{25}$$

Clearly there are many micromaxima per peak of the macroscopic process. The two distinct regions of the power spectral density permit an easy decomposition of the wall processes $y(t)$, $\dot{y}(t)$, and $\ddot{y}(t)$ into macroscopic (low frequency) and microscopic (high frequency) components. For a problem with a continuous power spectral density, a smoothing filter as examined by Crandall[18] may be used for the decomposition.

The decomposition of the Gaussian signal yields two independent random processes[21]

$$E\{\bar{y}(t)\ d(t)\} = 0 \qquad \sigma_y^2 = \sigma_{\bar{y}}^2 + \sigma_d^2$$

$$E\{\dot{\bar{y}}(t)\ \dot{d}(t)\} = 0 \qquad \sigma_{\dot{y}}^2 = \sigma_{\dot{\bar{y}}}^2 + \sigma_{\dot{d}}^2$$

$$E\{\ddot{\bar{y}}(t)\ \ddot{d}(t)\} = 0 \qquad \sigma_{\ddot{y}}^2 = \sigma_{\ddot{\bar{y}}}^2 + \sigma_{\ddot{d}}^2 \tag{26}$$

with

$$\sigma_{\bar{y}} = 0.16503623 \times 10^1 \text{ m} \qquad \sigma_d = 0.63558716 \times 10^{-4} \text{ m}$$

$$\sigma_{\dot{\bar{y}}} = 0.19030049 \times 10^{-2} \text{ m/s} \qquad \sigma_{\dot{d}} = 0.44024768 \times 10^{-3} \text{ m/s}$$

$$\sigma_{\ddot{\bar{y}}} = 0.25429066 \times 10^{-5} \text{ m/s}^2 \qquad \sigma_{\ddot{d}} = 0.16143511 \times 10^{-1} \text{ m/s}^2 \tag{27}$$

The resulting upcrossing and maxima frequencies are

$$\nu_{\bar{y}} = 0.18351888 \times 10^{-3} \qquad \nu_d = 0.11024073 \times 10^1$$

$$\mu_{\bar{y}} = 0.21267216 \times 10^{-3} \qquad \mu_d = 0.58360775 \times 10^{-1}$$

$$\mu_{\bar{y}}/\nu_{\bar{y}} = 0.11588571 \times 10^1 \qquad \mu_d/\nu_d = 5.2939393 \tag{28}$$

Therefore, the smoothed wall process has an average of 1.158857 maxima per upcrossing (or cycle). Since this is close to one, the wall process geometry closely resembles Fig. 5 and the lower bound will be tight. Further note that

$$\sigma_{\bar{y}}/\sigma_y \cong 1.0 \qquad \nu_{\bar{y}}/\nu_y = 0.97426848 \tag{29}$$

Thus, the smoothed process retains nearly all of the signal's amplitude and has on average fewer cycles per unit time. The apparent drop in "frequency" is due to wall process smoothing removing spurious microcycles. Therefore, the decomposition does not alter the original signal's significant maxima amplitude-time characteristics. Finally, unless the maximum stroke is of the same magnitude as the microscopic component, the smoothed wall acceleration $\ddot{\bar{y}}(t)$ establishes an upper bound $\sigma_{\ddot{\bar{y}}}$ on the minimum root-mean-square experiment acceleration.

With the significant maxima distribution found, attention is now turned to finding the needed first-passage time moment. The low frequency part of the power spectral density, Eq. (23), is converted to an equivalent dynamical system via

spectral factorization yielding the shaping filter

$$G_{\bar{y}}(s) = \frac{8.64581}{(s/0.00116)^2 + 0.1(s/0.001160) + 1} \tag{30}$$

with a bandlimited white noise excitation $n(t)$ described by

$$S_n(\omega) = \begin{cases} 1 & 0 \le \omega \le 0.006283 \\ 0 & 0.006283 < \omega \end{cases} \tag{31}$$

Converting Eq. (30) into two first order differential equations produces

$$\dot{\bar{y}}_1 = \bar{y}_2 \tag{32a}$$

$$\dot{\bar{y}}_2 = -1.3456 \times 10^{-6}\bar{y}_1 - 1.16 \times 10^{-4}\bar{y}_2 + 1.16338 \times 10^{-5}\, n \tag{32b}$$

with initial conditions from Eqs. (15) and (22)

$$\bar{y}_1(0) = \bar{y}_{1_0} = z + L/2$$

$$\bar{y}_2(0) = 0 \tag{33}$$

The bandlimited white noise process $n(t)$ is approximated by the sum of a large number of sinusoids at nearly evenly spaced frequencies between zero and the cutoff frequency via the method advocated by Shinozuka and Jan.[27] The phases are random while the amplitudes are determined by the power spectral density desired. As the number of sinusoids is increased, the approximated signal approaches $n(t)$. It was determined through testing that 40 was a sufficient number of sinusoids for this example.

The differential equations of Eq. (32) are numerically integrated from the initial conditions until the first crossing. If the process rises above the initial position $\bar{y}_{1_0}$, the simulation is stopped and restarted from the initial condition again. This insures that the crossing time obtained is the first-passage time from the maxima. The first-passage time of each simulation is recorded, and the fourth moment of T^{-1} is calculated from the collection of k first-passage times

$$m_{-4}(\bar{y}_{1_0}) = \frac{1}{k}\sum_{i=1}^{k} T_i^{-4} \tag{34}$$

For an ergodic process,[16] as the sample size k grows, this statistic approaches $E\{T^{-4}|\bar{y}_{1_0}\}$. The statistic $m_{-4}(\bar{y}_{1_0})$ is found for a range of $\bar{y}_{1_0}$ values. The results of the simulations for the example are shown in Fig. 10. Note that the data are asymptotic to

$$\left[\omega_d / \tan^{-1}\left(\frac{-\sqrt{1-\xi^2}}{\xi}\right)\right]^4 = 0.26105 \times 10^{-12}\ \mathrm{s}^{-4}$$

as $\bar{y}_{1_0}$ approaches infinity where ω_d is the damped natural frequency of Eq. (32). This is because the noise is essentially negligible when the system's energy is very high. Once the maximum stroke L is specified, the $E\{T^{-4}|\bar{y}_{1_0}\}$ yields the $E\{T^{-4}|z\}$. The data points are cubic spline interpolated to provide an approximation of the function $E(T^{-4}|z)$ suitable for numerical integration.

The experiment acceleration mean square lower bound sought can now be calculated from the significant maximum probability density and the conditional moment on the first-passage time by numerical quadrature of Eq. (7) using Eqs. (16), (19), and (28) along with the interpolation of the inverse moment data. This is done for varying values of maximum stroke. The lower bound on minimum root-mean-square experiment acceleration that can be obtained under prolonged exposure to the example vibration environment given the stroke constraint is thus computed and is plotted in Fig. 11 vs maximum stroke. For example, with a maximum stroke of 1 m, according to the figure the root-mean-square acceleration of an experiment must be greater than 0.17 μg, whereas if a 2-m stroke is permitted, this can be reduced to 0.13 μg. Note that the lower bound is non-zero for finite maximum stroke. This is in contrast to the previously reported results for harmonic disturbances where the maximum acceleration was zero when the maximum stroke was greater than twice the harmonic amplitude.

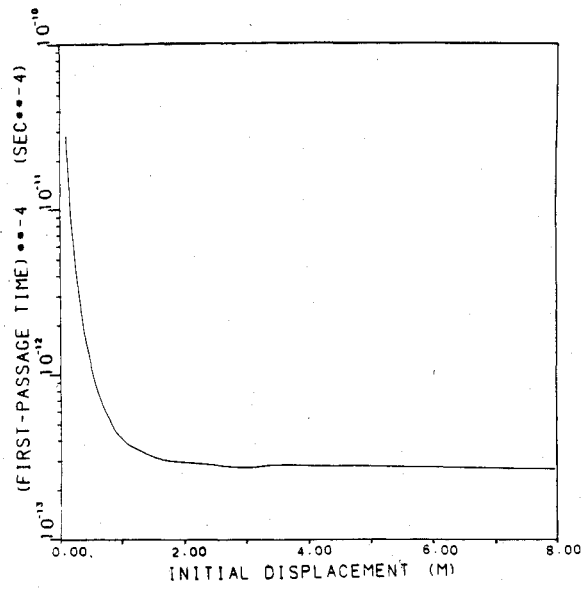

Fig. 10 Numerically computed fourth moments of T^{-1}.

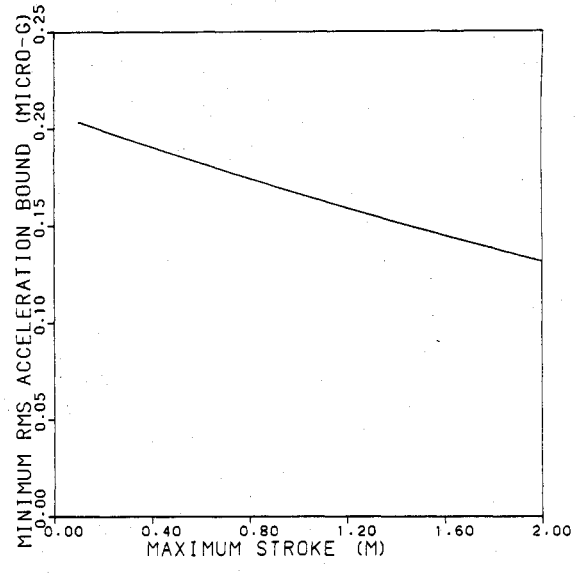

Fig. 11 Lower bound on root-mean-square experiment acceleration under prolonged exposure to specified vibration environment.

Conclusions

In this paper, the microgravity vibration isolation problem was formulated as a one-dimensional kinematic problem. The geometry of the stochastic wall trajectories was defined in terms of their significant extrema. An optimal control solution for the minimum acceleration return path determined a lower bound on experiment mean-square acceleration. This bound

was expressed in terms of the probability density function on the significant maxima and the conditional fourth moment of the first passage time inverse. For an example given, the first of these was found analytically while the second was found via Monte Carlo simulation. The experiment root-mean-square acceleration lower bound as a function of available space was then determined through numerical quadrature.

The method of analysis is quite general and intuitive. The authors feel that this could be applied to other problems with stochastic constraints. While such an analysis does not yield a controller, it does aid in the selection of system parameters (for example, the maximum stroke).

Lower bound plots of the type developed here may assist microgravity experiment designers as well as vibration isolation engineers. The lower bound depicted in plots of this type could not be achieved by real systems for several reasons. The levels derived are beneath the theoretical minimums. In addition, a real system is causal and cannot base its current control on unknown future disturbances. Also, any real active control system will have some non-ideal characteristics. The sensors employed to provide feedback will have some error as well. In spite of these comments, the authors of this paper are optimistic about attaining microgravity isolation levels close to the levels depicted here with an active vibration isolation system.

Appendix A: Solution for Optimal Trajectory

The derivation of the optimal trajectory proceeds as follows. Define the system state variables as

$$x_1 = x \qquad \dot{x}_1 = x_2 \qquad \dot{x}_2 = u \tag{A1}$$

and the equations of motion become

$$\dot{\boldsymbol{x}} = \boldsymbol{A}\boldsymbol{x} + \boldsymbol{B}u$$

$$\boldsymbol{x}^T = [x_1\ x_2] \qquad A = \begin{bmatrix} 0 & 1 \\ 0 & 0 \end{bmatrix} \qquad B^T = [\,0\ \ 1\,] \tag{A2}$$

The cost function is adjoined by the equations of motion and the final condition, utilizing three Lagrange multipliers.[14] The result is

$$J = \phi x_{1_f} = \int_{t_1}^{t_2} [u^2 + \lambda_1(x_2 - \dot{x}_1) + \lambda_2(u - \dot{x}_2)]\ \mathrm{d}t \tag{A3}$$

which is the general functional for this problem. Define the Hamiltonian and final condition cost[14] as

$$H = u^2 + \lambda_1 x_2 + \lambda_2 u \qquad G = \phi x_{1_f} \tag{A4}$$

Employing the calculus of variations, the minimization equations are

$$\dot{\lambda}_1 \equiv \frac{\partial H}{\partial x_1} = 0 \qquad \dot{\lambda}_2 \equiv -\frac{\partial H}{\partial x_2} = -\lambda_1 \qquad 0 \equiv \frac{\partial H}{\partial u} = 2u + \lambda_2 \tag{A5}$$

with natural boundary conditions

$$\lambda_{1_f} = G_{x_{1_f}} = \phi, \qquad \lambda_{2_f} = G_{x_{2_f}} = 0 \tag{A6}$$

Solving this gives

$$\lambda_1 = C_0, \qquad \lambda_2 = -C_0 t + C_1, \qquad u = \tfrac{1}{2} C_0 t - \tfrac{1}{2} C_1 \tag{A7}$$

Imposing the prescribed and natural boundary conditions yields

$$C_0 = \frac{6z}{T^3}, \qquad C_1 = \frac{6zt_2}{T^3} \tag{A8}$$

and

$$u(t) = \frac{3z}{T^3} t - \frac{3z}{T^3} t_2$$

$$\dot{x}(t) = \frac{(3/2)z}{T^3} t^2 - \frac{3zt_2}{T^3} t - \frac{(3/2)z(t_1^2 - 2t_2t_1)}{T^3}$$

$$x(t) = \frac{(1/2)z}{T^3} t^3 - \frac{(3/2)zt_2}{T^3} t^2 - \frac{(3/2)z(t_1^2 - 2t_2t_1)}{T^3} t + \frac{(1/2)z(2t_2^3 - 6t_1t_2^2 + 3t_1^2t_2)}{T^3} \tag{A9}$$

where $T = (t_2 - t_1)$, the time from significant extrema to zero crossing, or the first-passage time.

Appendix B: Shaping Filter for Simulation

The power spectral density is first approximated by a rational polynomial in ω^2. (This can be done to any required accuracy for a given power spectral density by using higher order polynomials.) This representation of the true power spectral density is then factored into two terms

$$S_{\ddot{y}}(\omega^2) = G(j\omega)G(-j\omega) \tag{B1}$$

The first term $G(j\omega)$ has all its poles and zeroes in the left half plane, whereas the poles and zeroes of the second term, $G(-j\omega)$, are the mirror images in the right half plane Replacing $j\omega$ in $G(j\omega)$ with the complex frequency variable s yields the transfer function that produces a Gaussian random process with power spectral density $S(\omega)$ from Gaussian white noise input:

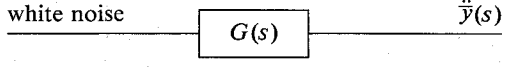

It is a straightforward process to convert the transfer function, or shaping filter, with n poles and m zeroes to $n + m$ first order linear differential equations with white noise input via the inverse Laplace transform and algebraic manipulation.[17,26] (Note that the derivative of white noise is nonexistent.) For most applications only the model of the low frequency component $\bar{y}(t)$ as a set of differential equations is needed to generate the $E\{(1/T^4)|z\}$.

Acknowledgment

This work was supported in part by NASA Lewis Research Center and the Commonwealth of Virginia.

References

[1]Spencer, L., "Overview of NASA Microgravity Programs and Opportunities," Vibration Isolation Technology for Microgravity Science Workshop, NASA Lewis Research Center, Sept. 1988.

[2]Alexander, J. I., "Experiment Sensitivity: Determination of Requirements for Isolation," Vibration Isolation Technology for Microgravity Science Workshop, NASA Lewis Research Center, Sept. 1988.

[3]Sharpe, A. (ed.), "Low Acceleration Characterization of Space Station Environment," Teledyne-Brown, Final Rept., SP85-MISFC-2928, Rev. B, NASA Marshall Space Flight Center, Oct. 1985.

[4]Stuhlinger, E., and Mookherji, T., "Materials Processing Twin Experiment," AIAA Paper 88-0348, Jan. 1988.

[5]Chassay, R. P., and Schwaniger, A. J., "Low-G Measurements by NASA," *Measurement and Characterization of the Acceleration Environment on Board the Space Station,* NASA Marshall Space Flight Center, Aug. 1986.

[6]Henderson, F., "MSL-2 Accelerometer Data Results," *Measurement and Characterization of the Acceleration Environment on Board the Space Station*, Teledyne-Brown, Aug. 1986.

[7]Grodsinsky, C. M., and Brown, J. V., "Low Frequency Vibration Isolation Technology for Microgravity Space Experiments," NASA

TM 101448, Sept. 1989.

[8]Fox, J. C., and McNally, P. J., "Current Orbiter Instrumentation and Acceleration Environment Data," Vibration Isolation Technology for Microgravity Science Workshop, NASA Lewis Research Center, Sept. 1988.

[9]Hamacher, H., Jilig, R., and Merbold, U., "The Microgravity Environment of the D-1 Mission," *Proceedings of the 37th IAF Conference,* Innsbruck, Austria, Paper IAF-86-268, 1986.

[10]Davis, L. P., Wilson, J. F., Jewell, R. E., and Roden, J. J., "Hubble Space Telescope Reaction Wheel Assembly Vibration Isolation System," Sperry Corp., Phoenix, AZ, March 1986.

[11]Wilson, J. F., and Davis, L. P., "Viscous Damped Space Structure for Reduced Jitter," 58th Shock and Vibration Symposium, Huntsville, AL, Aug. 1987.

[12]Hamilton, B. J., Andrus, J. H., and Carter, D. R., "Pointing Mount with Active Vibration Isolation for Large Payloads," AAS 87-033, Jan. 1987.

[13]Knospe, C. R., and Allaire, P. E., "Limitations on Vibration Isolation for Microgravity Space Experiments," *Journal of Spacecraft and Rockets,* Vol. 27, No. 6, pp. 642–646.

[14]Bryson, A. E., and Ho, Y.-C., *Applied Optimal Control: Optimization Estimation and Control*, Hemisphere, New York, 1975, Chaps. 2 and 3.

[15]Papoulis, A., *Probability, Random Variables, and Stochastic Processes*, McGraw-Hill, New York, 1984, Chaps. 5, 10, and 11.

[16]Newland, D. E., *An Introduction to Random Vibration and Spectral Analysis*, 2nd ed., Longman, New York, 1984, Chaps. 4 and 5.

[17]Brown, R. G., *Introduction to Random Signal Analysis and Kalman Filtering,* Wiley, New York, 1983, Chaps. 2 and 3.

[18]Crandall, S. H., "Distribution of Maxima in the Response of an Oscillator to Random Excitation," *Journal of the Acoustical Society of America,* Vol. 47, No. 3, March 1970, pp. 838–845.

[19]Rice, S. O., "Mathematical Analysis of Random Noise," *Bell System Technical Journal,* Vol. 23, 1944, pp. 282–332, Vol. 24, 1945, pp. 46–156.

[20]Huston, W. B., and Skopinski, T. H., "Probability and Frequency Characteristics of Some Flight Buffet Loads," NACA TN 3733, Aug. 1956.

[21]Lin, Y. K., *Probabilistic Theory of Structural Dynamics*, McGraw Hill, New York, 1967, Chap. 9.

[22]Crandall, S. H., and Mark, W. D., *Random Vibration in Mechanical Systems*, Academic Press, New York, 1963, Chap. 1.

[23]Roberts, J. B., "An Approach to the First-Passage Problem in Random Vibration," *Journal of Sound and Vibration,* Vol. 8, Jan. 1968, pp. 301-328.

[24]Vanmarcke, E. H., "On the Distribution of the First-Passage Time for Normal Stationary Random Processes," *Journal of Applied Mechanics,* Vol. 42, March 1975, pp. 215–220.

[25]Crandall, S. H., Chandiramani, K. L., and Cook, R. G., "Some First-Passage Problems in Random Vibration," *Journal of Applied Mechanics,* Vol. 33, pp. 532-538, Sept. 1966.

[26]Maybeck, P. S., *Stochastic Models Estimation, and Control*, Vol. 1, Academic Press, Orlando, FL, 1979, pp. 180–194.

[27]Shinozuka, M., and Jan, C.-M., "Digital Simulation of Random Processes and Its Applications," *Journal of Sound and Vibration,* Vol. 25, Jan. 1972, pp. 111–128.

Earl A. Thornton
Associate Editor